IEEE Access
Multidisciplinary ⋮ Rapid Review ⋮ Open Access Journal

Received March 15, 2021, accepted April 1, 2021, date of publication April 6, 2021, date of current version April 15, 2021.

Digital Object Identifier 10.1109/ACCESS.2021.3071344

Optimal Online Resonance Suppression in a Drive System Based on a Multifrequency Fast Search Algorithm

JIAKUAN XIA, ZHIYAN GUO, AND ZEXING LI

School of Electrical Engineering, Shenyang University of Technology, Shenyang 110870, China

Corresponding author: Zhiyan Guo (zhiyan_guo@163.com)

This work was supported in part by the National Natural Science Foundation of China under Grant 11971411 and Grant 52077142, in part by the University Innovation Team Project of Liaoning Province under Grant LT2013006, and in part by the Natural Science Foundation of Liaoning Province Education Department under Grant LJC201914.

ABSTRACT The resonant frequency drift caused by the change in mechanical parameters will cause the servo mechanism of CNC machine tools, robots and other equipment to produce mechanical resonance again. To address this problem, we propose a novel identification method of mechanical resonance based on the Fibonacci principle and a novel design method of notch filters based on optimization theory. First, by using a multifrequency sinusoidal signal, we design a fast search algorithm to search for the drift resonance frequency online; then, we optimize the notch filter to achieve fast and real-time resonance suppression by optimization theory. Compared with commonly employed passive resonance suppression methods, the proposed method can rapidly identify the parameters, more accurately suppress the resonance, minimize the phase angle loss and maintain the stability of the system. Finally, we apply the method to a 2-mass system experimental platform. The experimental results show that the proposed method is superior to the conventional passive resonant suppression method under the resonant frequency drift and other states and has strong robust performance.

INDEX TERMS Servo mechanism, mechanical resonance frequency drifts, Fibonacci principle, optimization theory, notch filter, phase angle loss.

I. INTRODUCTION

Permanent magnet synchronous motor (PMSM) drive systems are widely used for the motion control of precision equipment such as computer numerical control (CNC) machine tools, industrial robots, large optical telescopes and radar due to their high precision, high efficiency and high power density [1]–[4]. However, the mechanical transmission mechanism between the motor and the load often includes elastic factors that lead to mechanical resonance and limit the bandwidth of the position and speed control loop [5], [6]. The stiffness coefficient, inertia ratio, damping and other variables in the transmission system change with increasing equipment service life, so they are difficult to accurately measure. These variables make it difficult to identify and suppress mechanical resonance frequency drift, so the performance of the PMSM servo system is limited.

The associate editor coordinating the review of this manuscript and approving it for publication was Qinfen Lu.

At present, the research methods of mechanical resonance suppression are mainly divided into two categories: active methods and passive methods. Active methods mainly realize resonance suppression by changing the mechanical structure or by actively using advanced algorithms [7]. The adaptive neural network algorithm is adopted in [8], and the adaptive sliding mode control method is adopted in [7]–[11], while the adaptive feedback controller is used in [12], and the model predictive control algorithm is adopted in [13]. However, the operations of the above intelligent control algorithms are complex and require a large system computing capacity, which limits large-scale industrial applications [11]. In [14], an adaptive vector method for estimating the unknown parameters of the motor provided a new approach for parameter identification and resonance suppression. In recent years, state feedback control has been widely used to suppress mechanical resonance, where the idea is to observe state variables that include the mechanical resonance frequency [15]–[17]. However, these methods often require

additional sensors, which increases the hardware cost, and the installation of sensors is limited. The proportional integral (PI) controller is designed by pole assignment in [18], [19], and the system performance is improved by assigning the damping coefficient of the transfer function of the closed-loop system. However, the axial torque oscillation cannot be suppressed in the saturation stage of the speed regulator. In [11], [20], and [21], the shaft torque is measured directly or the displacement, speed and acceleration data of the load side are measured to obtain the resonance frequency and peak value, and then the mechanical resonance is suppressed by adjusting the controller parameters. These methods also increase the complexity and control cost of the system.

Passive methods do not change the control structure, do not increase the hardware cost, and are easy to implement. At present, the main passive resonance suppression method is the notch filter method [22]–[25]. However, this method needs to accurately identify the resonance frequency and peak value in real time. The offline suppression method is adopted in [26], [27]: the system Bode diagram obtained by the frequency sweep is analyzed, and then the filter parameters are set according to the characteristics of the resonance frequency. This method can accurately identify the resonance frequency. However, changes in the stiffness coefficient, inertia ratio and damping lead to changes in the resonance frequency and peak value, which leads to resonance suppression failure. However, the online real-time resonance suppression method can effectively prevent this problem.

In this paper, the mechanical resonance frequency drift of a servo system is studied as follows: 1) The mechanical resonance model of a PMSM servo system is established through the dynamic equation, and the frequency characteristics and phenomenon of the mechanical resonance drift of the system are analyzed. 2) Two iterative algorithms, including multifrequency fast search and fast multifrequency dichotomy, are given. The resonance frequency and cutoff frequency can be identified quickly and accurately online, and then the parameters of the resonant system of the drift can be determined. 3) By using the frequency characteristics of the system, the parameters of the notch filter are optimized and designed to achieve optimal online resonance suppression and keep the system stable. 4) The experimental results for the PMSM servo system are given to verify the correctness of the theoretical analysis and the effectiveness of the proposed method. Compared with the traditional offline resonance suppression method, the optimal online resonance suppression algorithm designed in this paper functions in real time and is fast, accurate, and stable.

The rest of this paper is arranged as follows. In section II, the model of the PMSM drive system is analyzed, the simplified model is deduced, and the influencing factors of mechanical resonance drift are analyzed. In section III, an optimal online mechanical resonance suppression scheme is proposed, and specific implementation steps are organized. The advantages of the method are illustrated by comparison with the offline method. The experimental results are given. Section IV presents the conclusion.

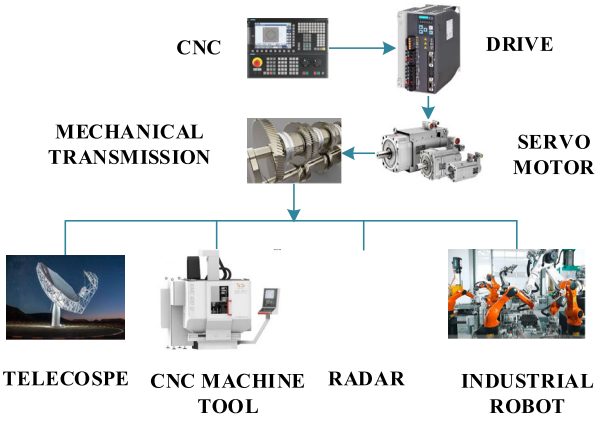

FIGURE 1. PMSM drive system.

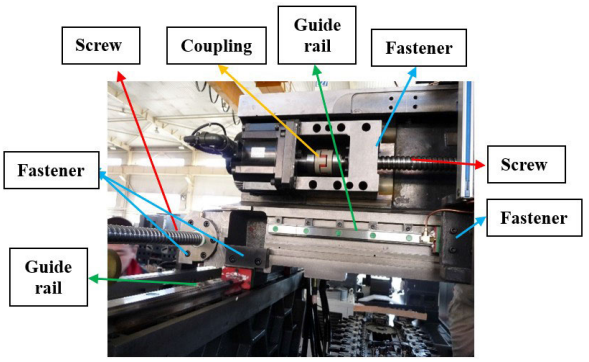

FIGURE 2. Mechanical transmission mechanism of the CNC machine.

II. MATHEMATICAL MODEL OF A PMSM DRIVE SYSTEM

In the practical application of industrial production, PMSM drive systems have been widely used, as shown in Fig. 1. The system is generally composed of a CNC system, servo driver, servo motor, mechanical transmission mechanism and load. Usually, the CNC system controls the output electromagnetic torque of servo motors by servo drivers, and the motor and load are connected by a mechanical transmission mechanism.

Fig. 2 shows that the mechanical transmission mechanism of the CNC machine tool includes screws, guide rails, a coupling, fasteners and other mechanical parts. The connection mode between these parts is not an ideal rigid connection but an elastic connection. The existence of elasticity introduces resonance points into the system and causes mechanical resonance.

A. ESTABLISHMENT OF A TWO-MASS MECHANICAL RESONANCE MODEL FOR THE PMSM SERVO SYSTEM

The typical two-mass mechanical model used to describe the servo system is shown in Fig. 3. The motor is connected to the load through a slender elastic shaft. The moments of inertia of the motor and the load are J_m and J_l, respectively, the stiffness

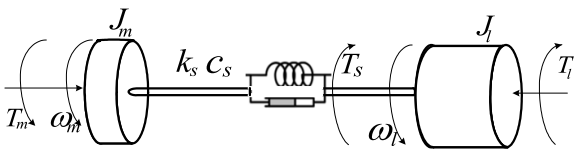

FIGURE 3. Two-mass model.

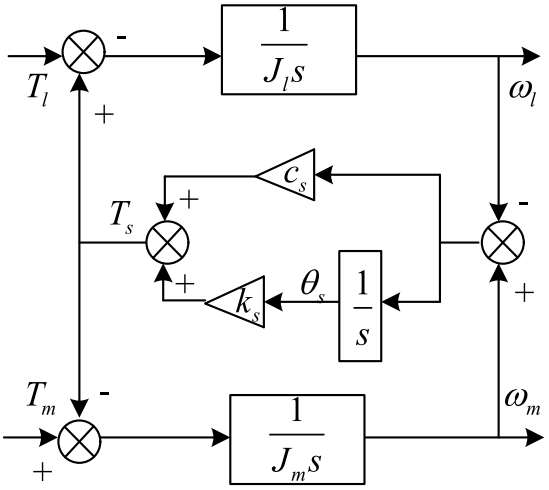

FIGURE 4. Block diagram of the two-mass model.

coefficient is k_s, the damping coefficient is c_s, the electromagnetic torque is T_m, the ratio of inertia is p, the disturbance torque is T_l, the shaft torque is T_s, ω_m and ω_l are the rotation speed of the motor and load, respectively, and θ_m and θ_l are their rotation angles, respectively. The kinematic equations of the system can be expressed as

$$\begin{cases} J_m\dot{\omega}_m = -T_s + T_m \\ J_l\dot{\omega}_l = T_s - T_l \\ T_s = k_s\left(\theta_m - \theta_l\right) + c_s\left(\omega_m - \omega_l\right) \\ \dot{\theta}_m = \omega_m \\ \dot{\theta}_l = \omega_l \\ \omega = 2\pi f \end{cases} \tag{1}$$

The block diagram of the two-mass mechanical model is shown in Fig. 4, where T_l is so small that it can be ignored. The transfer function from T_m to ω_m can be expressed as

$$G\left(s\right) = \frac{\omega_m}{T_m} = \frac{1}{J_m s} G_r\left(s\right) \tag{2}$$

$$G_r\left(s\right) = \frac{s^2 + 2k\xi_r\omega_{an}s + k\omega_{an}^2}{s^2 + 2\xi_r\omega_n s + \omega_n^2} \tag{3}$$

$G_r(s)$ is the transfer function of the mechanical resonance link of the servo system. ω_n and ω_{an} are the undamped resonance frequency and antiresonance frequency, respectively, which can be expressed as

$$\omega_n = \sqrt{\frac{k_s\left(1+p\right)}{J_m p}} \tag{4}$$

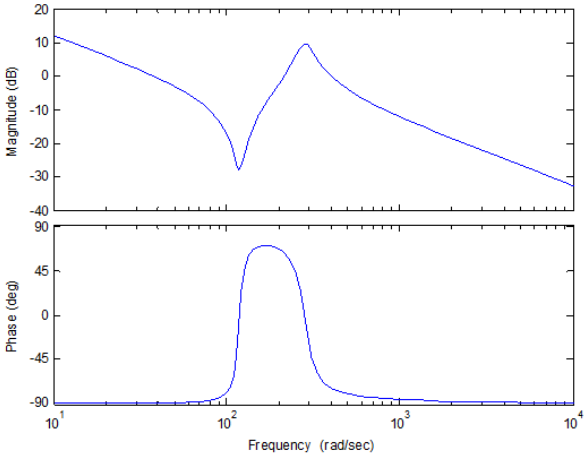

FIGURE 5. Bode diagram of the two-mass model.

$$\omega_{an} = \sqrt{\frac{k_s}{pJ_m}} \tag{5}$$

However, a change in the damping also causes drift of the resonance frequency, especially in some cases of servo precision control.

Let

$$k = \frac{1}{1+p} \tag{6}$$

$$\xi_r = \sqrt{\frac{c_s^2\left(1+p\right)}{4k_s J_m p}} \tag{7}$$

The damped resonance frequency and antiresonance frequency are ω_r and ω_{ar}, respectively. The relationship between ω_r and ω_n is given as follows:

$$\omega_r = \sqrt{\frac{\left(1+k\right) + \sqrt{\left(1-k\right)^2 + 8\xi_r^2 k + 8\xi_r^2 k^2}}{2 - 4\xi_r^2 - 4k\xi_r^2}}\omega_n \tag{8}$$

The relationship between ω_{ar} and ω_{an} is given as follows:

$$\omega_{ar} = \sqrt{\frac{\left(1+k\right) - \sqrt{\left(1-k\right)^2 + 8\xi_r^2 k + 8\xi_r^2 k^2}}{2k - 4k\xi_r^2 - 4k\xi_r^2}}\omega_{an} \tag{9}$$

By frequency domain analysis according to equation (2), the frequency characteristic curve of the mechanical resonance link of the servo system is obtained, as shown in Fig. 5.

B. ANALYSIS OF THE PHENOMENON OF MECHANICAL RESONANCE DRIFT

According to equations (4), (5), (8) and (9), the resonance frequency and antiresonance frequency are affected by the inertia ratio, stiffness coefficient and damping coefficient. The change in these three factors leads to drift in the resonance frequency. Therefore, the causes of resonance frequency drift can be summarized into three aspects: 1) The stiffness of the moving shaft is fixed in theory, but with increasing service life of the equipment, the aging of metal materials leads to a decrease in the stiffness coefficient; 2) in the process of

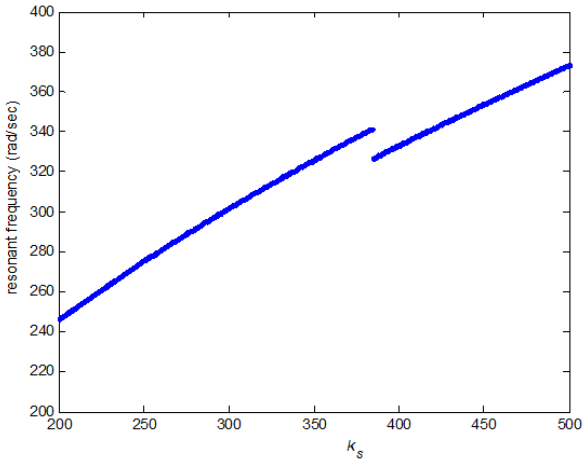

FIGURE 6. Curve of the resonance frequency with c_s.

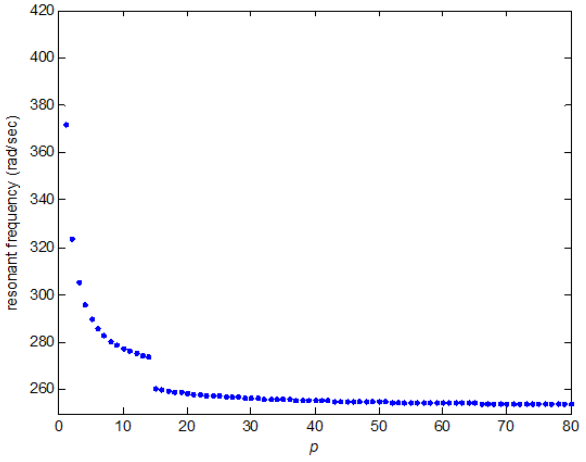

FIGURE 7. The curve of the resonance frequency with p.

using the equipment, a change in the preload and lubrication state of the transmission mechanism leads to a change in the damping coefficient; 3) in the working process of the CNC machine tools and industrial robots, a change in the load leads to a change in the inertia ratio. This paper discusses the influence of the simultaneous variation in the inertia ratio, stiffness coefficient and damping coefficient on the frequency drift of the mechanical resonance. According to the actual mechanical characteristics of CNC machine tools, the following assumptions need to be satisfied: $0 \leq c_s \leq 1$, $1 \leq p \leq 20$, and $200 \leq k_s \leq 500$. In addition, the initial values of other mechanical parameters are established as follows: $J_m = 0.043kg \cdot m^2$, $J_l = 0.22kg \cdot m^2$, $k_s = 280N \cdot m/rad$, and $c_s = 0.22N \cdot m \cdot s/rad$.

1) ANALYSIS OF THE VARIATION IN THE STIFFNESS COEFFICIENT

As shown in Fig. 6, when the inertia ratio p and the damping coefficient c_s remain unchanged and only the stiffness coefficient changes, the resonance frequency point changes. With a gradual increase in k_s, the resonance frequency of the system ω_r increases in a piecewise manner. When $k_s = 384N \cdot m/rad$, $\omega_r = 341.4803rad/s$; when $k_s = 385N \cdot m/rad$, $\omega_r = 326.8834rad/s$.

The resonance frequency jumps at a certain point. The interval [200, 500] is divided into two subintervals [200, 384] and [385,500]. The function fitted by the least square method is two straight lines expressed as

$$\begin{cases} \omega_r = 0.5142k_s + 146.3961 & k_s \in [200, 384] \\ \omega_r = 0.4032k_s + 172.1765 & k_s \in [385, 500] \end{cases} \tag{10}$$

The fitting correlation coefficient reaches 0.9999.

2) ANALYSIS OF THE VARIATION IN THE INERTIA RATIO

As shown in Fig. 7, when the stiffness coefficient c_s and the damping coefficient c_s remain unchanged, only the inertia ratio changes, and the resonance frequency point changes. With the gradual increase in p, the resonance frequency ω_r decreases in a piecewise manner, and the interval [0, 80] is divided into two subintervals [0, 14] and [15, 80]. When $p = 14$, the resonance frequency ω_r jumps. The function fitted by the least square method is given as

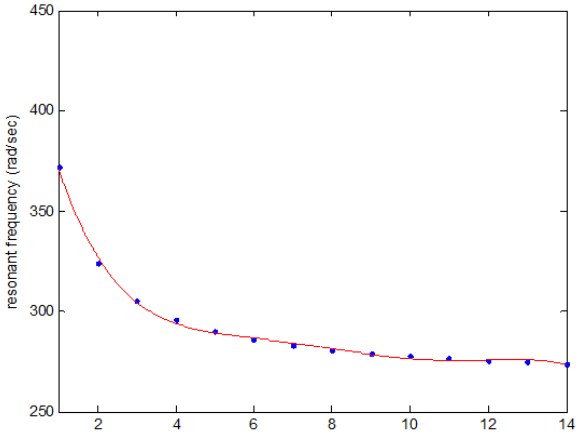

FIGURE 8. Fitting curve of the resonance frequency ($p \in [0, 14]$).

$$\begin{cases} \omega_r = -0.0042\,p^5 + 0.1818\,p^4 - 3.0468\,p^3 \\ \qquad + 24.6396\,p^2 - 98.6696\,p + 447.6226 \\ p \in [1, 14] \\ \omega_r = -0.0003\,p^3 + 0.0228\,p^2 - 0.9299\,p \\ \qquad + 270.1689 \\ p \in [15, 80] \end{cases} \tag{11}$$

The fitting curves are shown in Fig. 8 and Fig. 9.

3) ANALYSIS OF THE VARIATION IN THE DAMPING COEFFICIENT

In most cases, the value of the damping coefficient is very small, and equations (8) and (9) can be rewritten as

$$\omega_r \approx \omega_n \tag{12}$$

$$\omega_{ar} \approx \omega_{an} \tag{13}$$

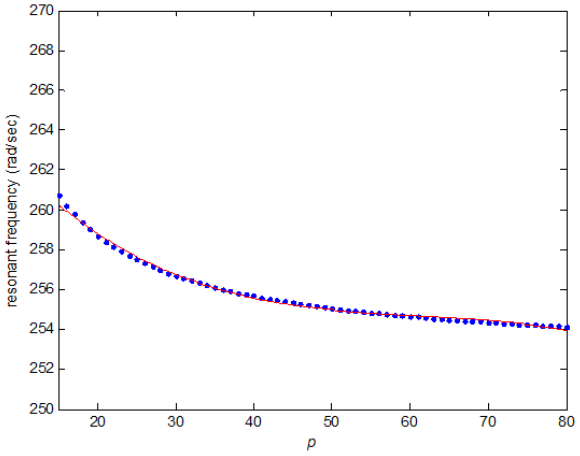

FIGURE 9. Fitting curve of the resonance frequency ($p \in [15, 80]$).

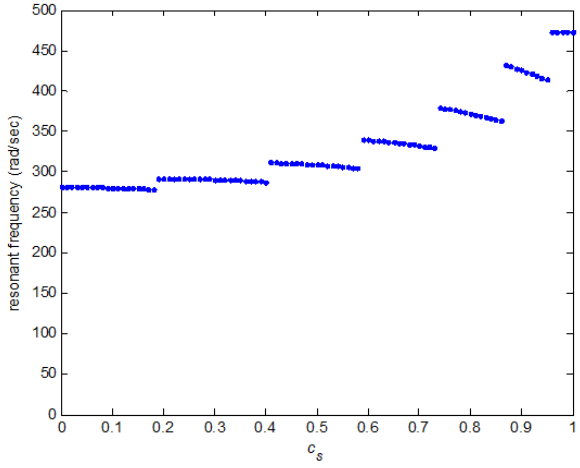

FIGURE 10. Curve of the resonance frequency with c_s.

This means that damping is ignored, but in some cases of precise control, damping can also affect the performance of the equipment. Fig. 10 shows the Bode diagram of the resonance frequency ω_r with varying c_s.

As shown in Fig. 10, with increasing c_s, the resonance frequency increases in a piecewise manner, and the interval [0,1] is divided into seven cells. By using the least squares method, we can calculate the correlation coefficient and linear relationship between the damping coefficient c_s and resonance frequency ω_r in each cell.

As shown in Table 1, with decreasing damping coefficient, the resonance frequency of the system drifts to the low-frequency region.

III. OPTIMAL ONLINE MECHANICAL RESONANCE SUPPRESSION SCHEME

From the above discussion, it can be seen that changes in the stiffness coefficient, inertia ratio and damping coefficient lead to resonance frequency drift, which causes the original resonance suppression method to fail. Aiming at the problem

TABLE 1. Relationship between ω_r^* and C_s.

c_s	ω_r^*	R	RELATIONSHIP
[0.000,0.189]	[278,282]	-0.9649	$\omega_r^* = -12.8168C_s + 281.6398$
[0.190,0.409]	[287,292]	-0.9431	$\omega_r^* = 17.3197C_s + 295.6660$
[0.410,0.589]	[304,312]	-0.9878	$\omega_r^* = 40.4683C_s + 328.8139$
[0.590,0.739]	[329,341]	-0.9952	$\omega_r^* = 75.6251C_s + 385.4153$
[0.740,0.869]	[363,380]	-0.9974	$\omega_r^* = 133.1312C_s + 478.6739$
[0.870,0.959]	[414,432]	-0.9990	$\omega_r^* = 220.9143C_s + 624.3694$
[0.960,1.000]	[473,474]	0	$\omega_r^* = 473.4979$

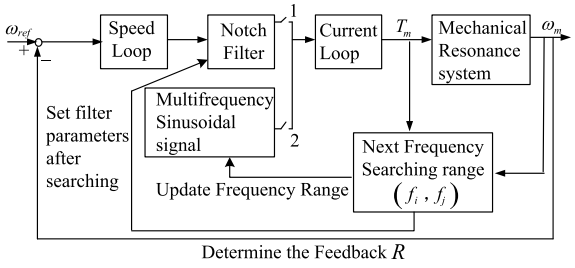

FIGURE 11. Block diagram of the search algorithm.

of the real-time control of resonance point drift, first, a fast interval searching iterative algorithm based on the Fibonacci principle is proposed to accurately detect the resonance frequency in real time. Second, a fast multifrequency bisection method is proposed to quickly and accurately obtain the cutoff frequency. Third, the threshold frequency is calculated to determine the parameters of the mechanical resonance system. Finally, the performance index function is constructed, the parameters of the notch filter are designed by using optimization theory, and then online optimal suppression for the mechanical resonance of the servo system is implemented. The control structure of the frequency characteristic search algorithm is shown in Fig. 11.

A. SEARCH ALGORITHM DESIGN OF THE RESONANCE FREQUENCY

The commonly used one-dimensional search methods can be divided into two categories: trial methods and interpolation methods. Because the interpolation method needs to obtain a smooth function and satisfy other conditions, the trial method needs only to obtain a function that is unimodal. In comparison, the trial method is simple and feasible. Based on the principle of the Fibonacci method, an iterative algorithm for fast searching intervals is proposed in this paper. The method is as follows. First, let $\varphi(\lambda)$ be the unimodal function. The interval $[\alpha, \beta]$ is inserted into n points $\lambda_1, \lambda_2, \cdots, \lambda_n$, and then the interval is equally divided into $n+1$ cells. We calculate the function value $\varphi(\lambda_i)$ $(i = 1, 2, \cdots, n)$ at each point.

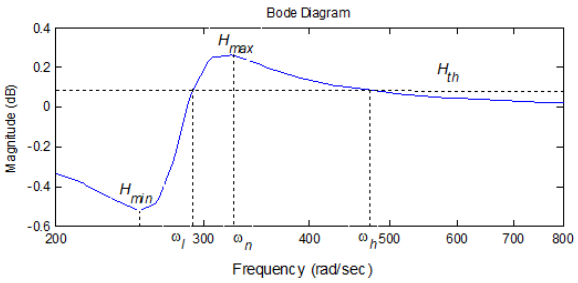

FIGURE 12. Bode diagram threshold analysis for the two-mass system.

There must be a maximum value point λ_r such that $\varphi(\lambda_r) \geq \varphi(\lambda_i)$ $(i = 1, 2, \cdots, n)$; then, we take the two adjacent points of λ_r, namely, λ_{r-1} and λ_{r+1}. Obviously, the maximum point must be in the interval $[\lambda_{r-1}, \lambda_{r+1}]$. Finally, the maximum value can be obtained by iteration. This method can quickly and accurately find the extremum of a single peak function. We use the multifrequency sinusoidal signal and Fibonacci method to search for the resonance frequency online, so this method is called the multifrequency fast search method. The specific measures are as follows.

1) DETERMINATION OF THE THRESHOLD

According to the variation ranges of the stiffness coefficient k_s, inertia ratio p and damping coefficient c_s, the search interval $[f_c, f_e]$ is determined such that the image in the search interval is a unimodal function. Here, $\omega = 2\pi f$, as shown in Fig. 12.

The setting of the threshold value is related to fast Fourier transform (FFT) sampling. Following Shannon's sampling theorem, 1024 points are used for the FFT analysis in the experiment. The threshold value is $H_{th} = 1.5$, and the threshold frequencies are f_l and f_h, corresponding to the angular frequencies ω_l and ω_h in Fig. 12. $H_{\max}$ is the maximum value, and $H_{\min}$ is the minimum value. If the amplitude of a certain frequency point exceeds the threshold, there is considered to be obvious resonance in the system. Let the amplitude of the two-mass system at the resonance frequency f be Q_f; the following expression can be obtained from equation (2):

$$Q_f = \frac{1}{2\pi f J_m} \sqrt{\frac{\left(f^2 - k f_r^2\right)^2 + (2k\xi_r f_r f)^2}{\left(f^2 - f_r^2\right)^2 + (2\xi_r f_r f)^2}} \tag{14}$$

where f_r is the resonance frequency found.

2) MULTIFREQUENCY SINUSOIDAL TORQUE CURRENT SIGNAL

It is assumed that the multifrequency sinusoidal torque current signal with online frequency variation is composed of n_0 sinusoidal signals with different frequencies. The frequency interval between each sinusoidal signal is $\tau = (f_e - f_c)/n_0$. The multifrequency sinusoidal torque current signal can be expressed by the following equation:

$$i_q(t) = \frac{i_{q\max}}{\xi n_0} \sum_{i=1}^{n_0} \sin\left[2\pi\left(f_c + i\tau\right)t\right] \tag{15}$$

where $i_{q\max}$ is the limiting amplitude of the motor torque current and ξ is the adjustment coefficient, which ensures that the motor speed runs in a safe range.

3) RESONANCE FREQUENCY SEARCH

Using the multifrequency sinusoidal torque current excitation system shown in (15), the motor speed and torque current are sampled and stored online. By using equation (2), it can be deduced that the amplitude gain K of the mechanical resonance of the two-mass system at frequency f is expressed as follows:

$$K = A_m / K_i A_{im} \tag{16}$$

where K_i is the motor torque coefficient, A_m and A_{im} are the amplitude of the motor angular speed and the amplitude of the torque current, respectively.

Fig. 12 shows that the amplitude gain K reaches the minimum value and maximum value at the antiresonance frequency and resonance frequency of the system, respectively. The multifrequency fast search algorithm searches for the minimum value and maximum value of K in the target frequency $[f_c, f_e]$, and then the resonance frequency characteristics of the system are obtained.

The process of the multifrequency fast search method for finding the characteristics of the resonance frequency is as follows:

① The initial interval is set as $[f_c, f_e]$; n_0, τ, ξ and $i_{q\max}$ are determined; and the accuracy requirement $\varepsilon = 1$;

② Using a multifrequency sinusoidal signal excitation system, the speed and torque current of the motor are transformed by FFT, and then A_m and A_{im} are obtained;

③ According to equation (16), the amplitude gain $K = K(f_c + i\tau)$ $(i = 1, \cdots, n_0)$ is determined, and the maximum point f_r of K is obtained;

④ If $f_{r+1} - f_{r-1} \leq \varepsilon$, the calculation is stopped; an appropriate point is taken as the approximate maximum point, and the corresponding function value is the approximate maximum value; otherwise, ⑤ is executed;

⑤ $f_c = f_{r-1}$, and $f_e = f_{r+1}$; the search restarts at ①.

Similarly, the antiresonance frequency can be obtained.

4) CUTOFF FREQUENCY SEARCH

Using the dichotomy and multifrequency sinusoidal signal, we propose an iterative algorithm for fast searching for a cutoff frequency referred to as fast multifrequency bisection. The common point of the two search algorithms mentioned above is that they are fast and easy to operate.

Let

$$h(f) = K - 1 \tag{17}$$

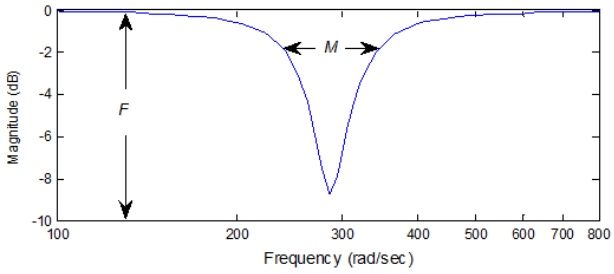

FIGURE 13. Amplitude-frequency response of the designed notch filter.

Then

$$h(f) = A_m / K_i A_{im} - 1 \tag{18}$$

The steps of the fast multifrequency bisection method for searching for the cutoff frequency are as follows:

Step ① and step ② are consistent with the above fast resonance frequency search algorithm.

③ According to (18), the amplitude gain is $h(f_c + i\tau)\,(i = 1, \cdots, n_0)$, and the value of $h(f_c + i\tau)$ is calculated.

④ If there is a frequency f_r that makes $h(f_r) = 0$, then the calculation stops; otherwise, ⑤ is executed.

⑤ The minimum frequency f_{r1} of $h(f_c + i\tau) > 0$ and the maximum frequency f_{r2} of $h(f_c + i\tau) < 0$ are determined. If $f_{r1} - f_{r2} \leq \varepsilon$, then the calculation stops, and an appropriate point is taken as the cutoff frequency; otherwise, ⑥ is executed.

⑥ $f_c = f_{r1}$, and $f_e = f_{r2}$; the search restarts at ①.

5) DETERMINATION OF THE THRESHOLD FREQUENCY AND DRIFT PARAMETERS

The mechanical resonance frequency, antiresonance frequency and cutoff frequency as well as their corresponding amplitudes A_{an}, A_n and 1 can be calculated by *A and B*. Let equation (14) be equal to A_{an}, A_n and 1, respectively. We have the coefficients k and ξ_r, the damping coefficient c_s, the inertia ratio p and the stiffness coefficient k_s. Let equation (14) be equal to H_{th}; finally, we obtain the frequency equal to the threshold value H_{th}.

B. OPTIMAL DESIGN OF THE NOTCH FILTER

To easily adjust the filter frequency, filter width and filter depth, an improved double-T network notch filter is adopted in this paper. Its transfer function is shown in equation (19), and the amplitude-frequency response characteristics are shown in Fig. 13. F is the amplitude gain of the notch filter at resonance frequency f_0, and M is the bandwidth. Obviously, when the depth f_0 and the width M are larger, the amplitude near the resonance frequency point can obtain sufficient attenuation. However, if these parameters are too large, it leads to excessive resonance suppression and reduces the stability margin of the servo system, resulting in obvious vibration in the system response. We need to determine how to select a and b to find the optimal depth and width parameters, limit the amplitude of the resonance frequency below the threshold value, and minimize the phase angle loss.

$$\begin{cases} G_N(s) = \dfrac{s^2 + 2\pi f_0 as + (2\pi f_0)^2}{s^2 + 2\pi f_0 bs + (2\pi f_0)^2} \\ F = \dfrac{a}{b} \\ M = 2\pi f_0 \sqrt{b^2 - 2a^2} \end{cases} \tag{19}$$

Mechanical resonance reduces the stability margin of the system, which not only affects the dynamic performance of the system but also destroys the stability of the system. Let the system be stable without a notch filter, and the phase margin of its open loop is φ_m, which can be expressed as

$$\begin{cases} \varphi_m = \arctan \dfrac{af_0 f}{f_0^2 - f^2} - \arctan \dfrac{bf_0 f}{f_0^2 - f^2}, & f \neq f_0 \\ 0 & f = f_0 \end{cases} \tag{20}$$

After the notch filter is added, the stability margin of the system is expressed as

$$\varphi_m^{new} = \varphi_m + \varphi$$

where φ is the phase angle loss at the shear frequency f_c, and the expression is

$$\varphi = \arctan \frac{af_0 f_c}{f_0^2 - f_c^2} - \arctan \frac{bf_0 f_c}{f_0^2 - f_c^2}, \quad f_0 > f_c \tag{21}$$

Let

$$\begin{cases} \varphi = \varphi_1 - \varphi_2 \\ \varphi_1 = \arctan \dfrac{af_0 f_c}{f_0^2 - f_c^2} \\ \varphi_2 = \arctan \dfrac{bf_0 f_c}{f_0^2 - f_c^2} \end{cases} \tag{22}$$

Then,

$$\begin{aligned} \tan\varphi &= \tan(\varphi_1 - \varphi_2) = \frac{\tan\varphi_1 - \tan\varphi_2}{1 + \tan\varphi_1 \tan\varphi_2} \\ &= \frac{(a-b)\frac{f_0 f_c}{f_0^2 - f_c^2}}{1 + ab\left(\frac{f_0 f_c}{f_0^2 - f_c^2}\right)^2} \end{aligned} \tag{23}$$

Let

$$m = \frac{f_0 f_c}{f_0^2 - f_c^2} \tag{24}$$

Then, (22) can be rewritten as

$$\varphi = are\tan \frac{(a-b)m}{1 + abm^2} \tag{25}$$

Since a is much smaller than b, the absolute value of (25) is taken as the phase angle loss caused at the cutoff frequency f_c; then, we have

$$|\varphi| = are\tan \frac{(b-a)m}{1 + abm^2} \tag{26}$$

Equation (26) shows that with a and b as the adjustment coefficients, the phase angle loss increases with decreasing a and vice versa, and the phase angle loss decreases with decreasing b and vice versa. Then, we can make the following conclusions. When b increases and a decreases, the depth of F and width of M increase, and the resonance suppression ability is enhanced. Simultaneously, the phase angle loss increases, which increases the influence on the stability of the system. When a increases and b decreases, the depth F and the width M decrease, and the resonance suppression ability decreases. Simultaneously, the phase angle loss decreases, and the influence on the stability of the system decreases. The final purpose of this paper is to select the optimal adjustment parameters a and b to minimize the phase angle loss, maintain the stability of the system, and effectively suppress the resonance.

Assuming the amplitude of the notch filter at frequency f is B_f, the expression obtained from equation (19) is presented as follows:

$$B_f = \sqrt{\frac{\left(f^2 - f_0^2\right)^2 + (af_0 f)^2}{\left(f^2 - f_0^2\right)^2 + (bf_0 f)^2}} \tag{27}$$

Obviously, B_f is a function of a and b and can be expressed as $B_f\ (a, b)$. For the threshold H_{th}, when $f < f_l, f > f_h$, $Q_f < H_{th}$; when $f_l \le f \le f_h$, $Q_f \ge H_{th}$. Therefore, we need only to consider that the amplitude corresponding to the interval $[f_l f_h]$ should be controlled below the threshold value H_{th}, and the amplitude of the other intervals should naturally be below the threshold value H_{th}; that is, equation (28) holds in the interval $[f_l f_h]$.

$$Q_f B_f \le H_{th} \tag{28}$$

With equation (28), we have the following optimal regulation parameters:

$$\min_{Q_f B_f \le H_{th}} |\varphi| = are\tan\frac{(b-a)m}{1+abm^2} \tag{29}$$

The specific steps of solving the optimization problem (29) with Zoutendijk's feasible direction method are presented as follows:

① The initial point is set to $x_1 = \left(\frac{a_1}{b_1}\right)$, and $k = 1$;

② The constraint formula (28) is recognized as $Ax_k \le \mathbf{0}$, where $A = \left[\frac{1}{2\pi f_r J_m}\sqrt{\frac{(1-k)^2+4k^2\xi_r^2}{4\xi_r^2}}H_{th}\right]$ and $x_k = \left(\frac{a_k}{b_k}\right)$;

③ Calculate $\nabla|\varphi(x_k)|$ Obtain the optimal solution p_k of the formula $\min_{Ax\le 0} \nabla|\varphi(x)|^T P$; $-1 \le p_i \le 1$, where $i = 1, \ldots, n$.

④ If $\nabla|\varphi(x_k)|p_k = \mathbf{0}$, the calculation is stopped; x_k is the Kuhn-Tucker point; otherwise, ⑤ is executed;

⑤ Obtain the optimal solution λ_k of the formula $\min_{st\ 0\le\lambda\le\lambda_{\max}} |\varphi(x_k + \lambda p_k)|$, where

$$\lambda_{\max} = \begin{cases} \min(\bar{c}_i/\bar{p}_i, \bar{p}_i) & \bar{p}_i > 0 \\ \infty & \bar{p}_i \le 0 \end{cases}, \quad \bar{c} = -Ax_k, p = Ap_k.$$

⑥ Set $x_{k+1} = x_k + \lambda_k p_k$, where $k = k + 1$.

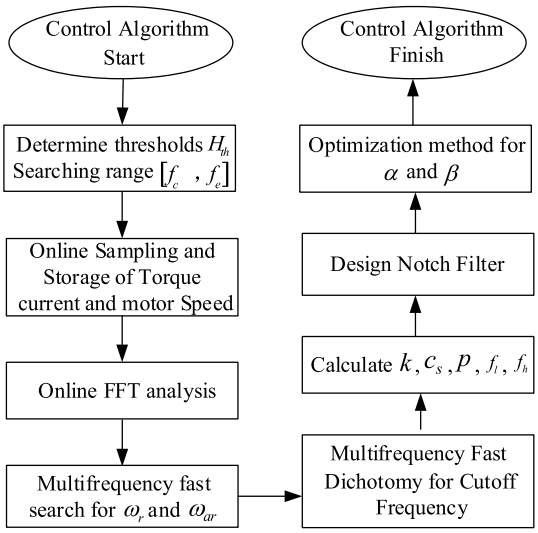

FIGURE 14. Flow chart of the optimal online resonant suppression algorithm.

The determined a and b can place the amplitude attenuation at any frequency ω in the resonant link below the threshold value H_{th}, and the phase angle loss is minimized to determine the optimal notch depth and notch width parameters, to avoid excessive suppression, and to maintain the stability of the system.

C. DESIGN OF THE OPTIMAL ONLINE RESONANCE SUPPRESSION ALGORITHM

The servo system resonance suppression scheme based on an adaptive notch filter mainly includes four steps: 1) data sampling, 2) FFT analysis, 3) resonance frequency fast search, and 4) notch filter parameter tuning. After the resonance online suppression function is turned on, the torque current signal is sampled. In each sampling period, the system completes data sampling, and at the same time, all the collected data are stored in the register. When the number of sampling points reaches the predetermined number, sampling is completed, and FFT analysis is carried out. The results of the FFT analysis are obtained by using the multifrequency fast search algorithm to obtain the resonance frequency and its amplitude gain. A notch filter is designed by using the resonance frequency and the parameters of the notch bandwidth and notch depth determined by optimization theory to realize online resonance suppression. The flow chart of the optimal online resonance suppression algorithm is shown in Fig. 14.

IV. EXPERIMENT

To verify that the optimal online resonance suppression algorithm can suppress the mechanical resonance frequency drift of the PMSM servo system in real time and maintain the stability of the system, an experimental device based on the two-mass elastic model is built, as shown in Fig. 15.

The experimental platform is mainly composed of a drive motor, load motor, damper, controller, and upper computer,

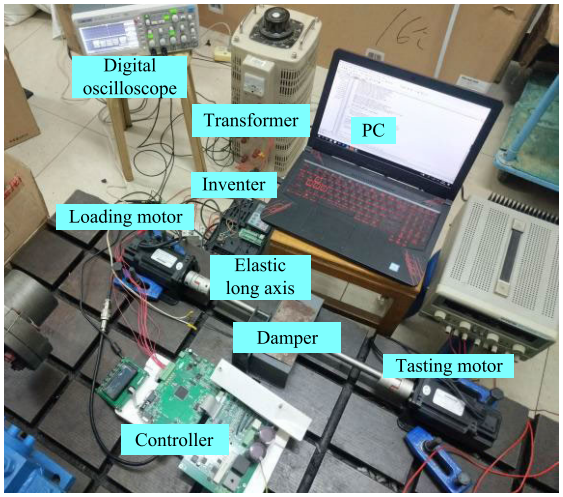

FIGURE 15. Experiment setup.

TABLE 2. Motor parameters used in the experiment.

Parameter	Units	Value
Rated Voltage (3-phase)	V	220
Rated Torque	N m	0.75
Max Torque	N m	2.4
Rated Revolution	r/min	7.2
Rotor Inertia	kg m²	1500
Rated Frequency	Hz	100

where the main chip of the controller is a TMS320F2812 of the TI company. C language is used for programming. The rated power of the permanent magnet synchronous motor is 750 W, and the switching frequency of the three-phase inverter is 10 kHz. The speed of the motor is obtained by a 2500 lines incremental encoder with itself, and the period of system speed loop is 0.45 ms. The drive motor and the load motor are connected by a slender elastic shaft. The motor parameters are shown in Table 2.

The load motor can provide different torques and obtain different moment of inertia ratios. The stiffness coefficient can be adjusted by changing different slender elastic shafts. The damping coefficient can be adjusted by adjusting the damper. When the three factors of the inertia ratio, stiffness coefficient and damping coefficient change at the same time, the experimental platform verifies the suppression effect of the optimal resonance suppression algorithm proposed in this paper and its influence on the stability of the servo system. Three experiments were carried out to verify the results. Experiment 1 verifies the suppression effect of the optimal online resonance suppression algorithm on mechanical resonance for the PMSM servo system. Experiment 2 verifies that the optimal online resonance suppression algorithm can still suppress the resonance in real time and keep the system stable after the resonance frequency drifts. Experiment 3 verifies that the optimal online resonance suppression algorithm has satisfactory robustness.

TABLE 3. Parameters used in the experiment.

Parameter	Initial value
J_m	0.043 kg m²
J_L	0.02 kg m²
K_i	2.35 N m / A
i_r	8.5 A
k_s	280 N m/rad
c_s	0.22 N m s/rad
p	4.6512

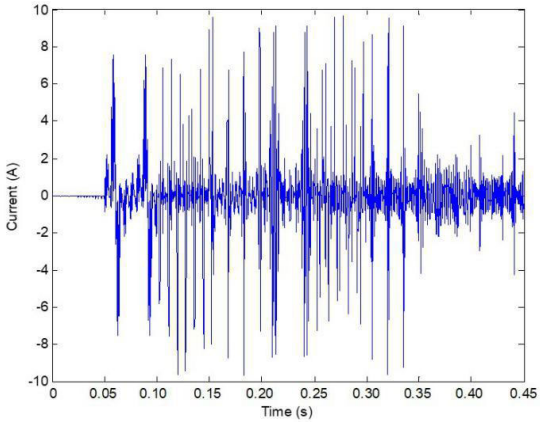

FIGURE 16. Response of the quadrature axis current in the multifrequency fast search procedure.

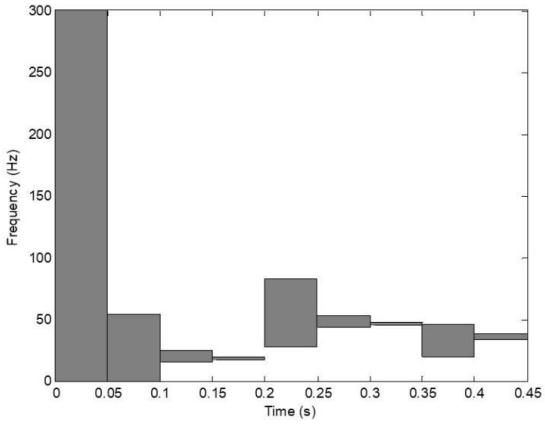

FIGURE 17. Updating process of the multifrequency fast search.

Experiment 1 Optimal online suppression of the resonance frequency

The initial mechanical parameters of the experimental platform are shown in Table 3. The optimal online resonance suppression method searches the resonance frequency online and automatically configures the filter. First, we initialize the multifrequency sinusoidal quadrature axis current signal, determine that the frequency search range $[f_c, f_e]$ is [0,300], and determine that the given speed is 500 r/min.

Fig. 16 shows the cross-axis current response over the whole search process, and Fig. 17 shows the iterative update process of the multifrequency fast search algorithm. The

TABLE 4. Parameters obtained from the search algorithm.

Symbol	Units	Value
f_r	Hz	45.4832
f_a	Hz	19.0947
K	dB	3.0459
f_c	Hz	34.6150
H_{th}	dB	3.5218
f_l	Hz	37.6152
f_h	Hz	55.5591

TABLE 5. Comparison of the phase margins before and after resonance suppression.

Condition	Phase margin
Before suppression	69.4300
General filter	63.5794
Optimized filter	69.2079

experimental results show that with 9 iterations, it takes 0.45 seconds to search for the resonance frequency f_r, the antiresonance frequency f_a, the amplitude gain K at the resonance frequency and the shear frequency f_c. The first seven iterations search for the resonance frequency and antiresonance frequency, which takes 0.35 seconds. The next two iterations search for the cutoff frequency, which takes 0.10 seconds. Then, the frequencies f_l and f_h corresponding to the threshold H_{th} are calculated by the algorithm. The results are shown in Table 4.

Both the fast search algorithm proposed in this paper and the search algorithm in [28] divide the search interval into 10 subintervals. The search algorithm in this paper can accurately determine each iteration interval with a small number of calculations and fast search speed, taking only 0.45 seconds, while the algorithm in [28] needs to judge and compare each subinterval to determine each iteration interval, so the number of calculations is large, taking 5.4 seconds to execute.

After the resonance frequency characteristics are identified by the fast search algorithm, the notch filter is automatically configured according to optimization theory. The performance index is established, and then the mechanical resonance amplitude is controlled below the threshold value, while the phase angle loss is minimized. The filter adjustment coefficients are determined to be $a = 0.1074$ and $b = 0.2949$. The simulation results are shown in Fig. 18, and the comparison of the phase margins is shown in Table 5. The results show that both the optimized notch filter and the ordinary notch filter can control the harmonic amplitude below the threshold value, but the less phase angle loss is caused by the optimized notch filter than by the ordinary notch filter. The optimized notch filter designed in this paper can minimize the loss of the phase angle and has little effect on the stability of the system.

Fig. 19 and Fig. 20 show the response waveforms of the motor quadrature axis current and motor speed of the servo system, respectively.

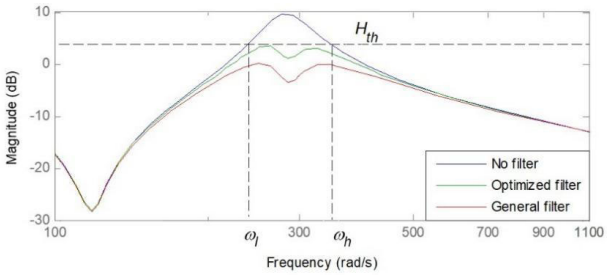

FIGURE 18. Simulation waveform of the two-mass system resonant suppression.

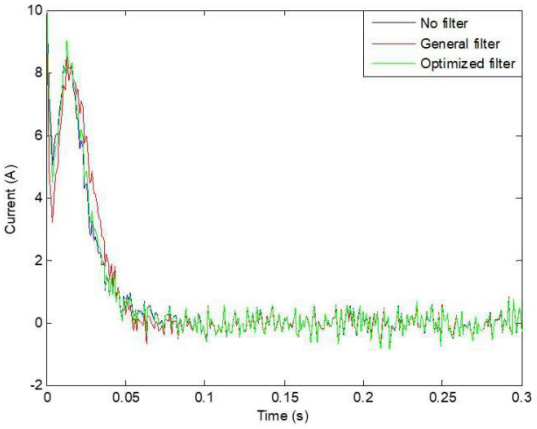

FIGURE 19. Quadrature axis current response.

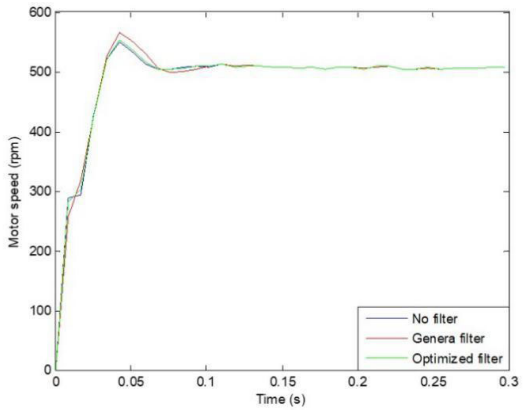

FIGURE 20. Motor speed response.

It can be seen that the optimal notch filter designed in this paper barely changes the stability of the system, while the ordinary filter causes obvious fluctuations in the speed response and current response. Manual adjustment of the notch filter parameters was used in [27], which takes a long time and makes it difficult to achieve an optimal effect. However, this paper establishes a real-time and accurate performance index to obtain the optimal adjustment parameters through the optimal algorithm.

Comparisons of the waveforms through FFT analysis of the quadrature axis current are shown in Fig. 21 and Fig. 22. It can

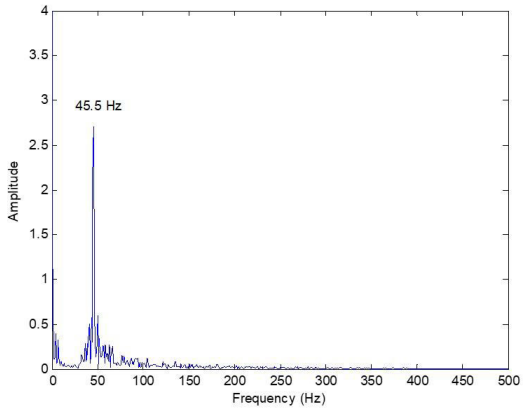

FIGURE 21. FFT analysis of the current waveforms before resonance suppression.

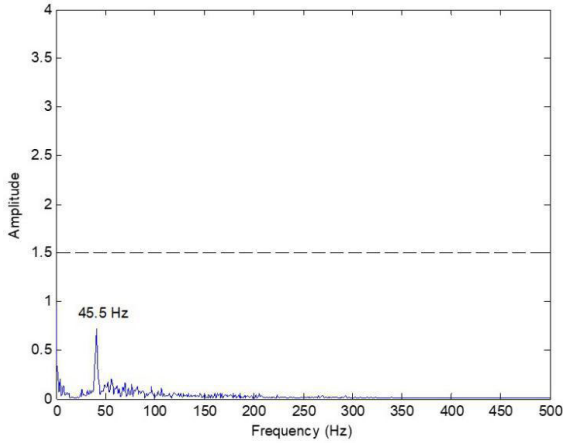

FIGURE 22. FFT analysis of the current waveforms after optimal online resonance suppression.

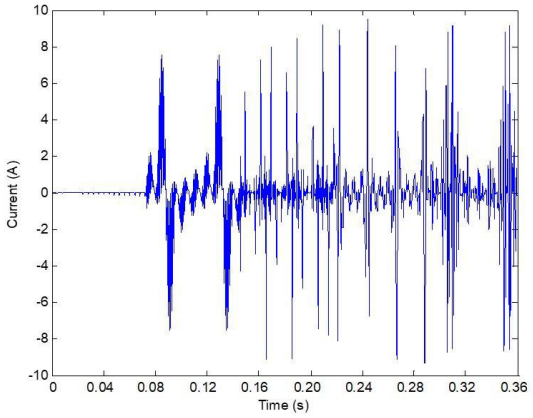

FIGURE 23. Response of the quadrature axis current in the multifrequency fast search procedure (resonance frequency drifts).

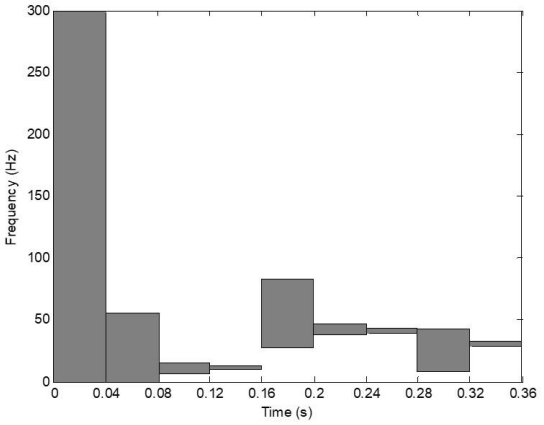

FIGURE 24. Updating process of the multifrequency fast search (resonance frequency drifts).

be seen that the optimized filter can significantly attenuate the mechanical resonance and keep it below the set threshold.

Experiment 2 Optimal online suppression after resonance frequency drift

The resonance frequency drifts because of changes in the stiffness coefficient, damping coefficient and inertia ratio due to replacement of the slender elastic shaft, adjustment of the damper and adjustment of the torque of the load motor, respectively. The resonance frequency f_r, antiresonance frequency f_a, amplitude gain K at the resonance frequency and shear frequency f_c can be identified by a multifrequency fast search algorithm. The response of the quadrature axis current in the search process is shown in Fig. 23, and the updating process of the multifrequency sinusoidal signal is shown in Fig. 24. Nine iterations take 0.36 seconds. The stiffness coefficient k_s, damping coefficient c_s, inertia ratio p and frequencies f_l and f_h corresponding to the threshold H_{th} are calculated by the algorithm. The results are shown in Table 6.

After the resonance frequency characteristics are identified by the fast search algorithm, the notch filter parameters are

TABLE 6. Parameters identified by the search algorithm.

Symbol	Units	Value
k_s	N m/rad	269
c_s	N m s/rad	0.17
p	—	20.0000
f_r	Hz	40.5774
f_a	Hz	9.2289
K	dB	0.0027
f_c	Hz	27.8356
f_l	Hz	31.3528
f_h	Hz	53.9249

optimized by experiment 1, with filter adjustment coefficients $a = 0.1202$ and $b = 0.5319$. The simulation results are shown in Fig. 25.

The contrast of the resonance suppression effect is very obvious. Fig. 26 shows the waveform of the resonance suppression by the general filter whose resonance suppression failure is caused by the resonance frequency drift.

Fig. 27 shows the waveform of the optimal online resonance suppression algorithm. The algorithm can effectively

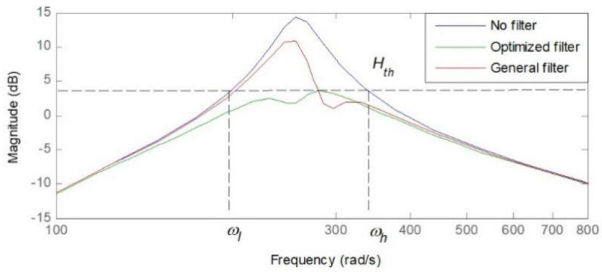

FIGURE 25. Simulation waveform of the 2-mass system resonant suppression (the resonance frequency drifts).

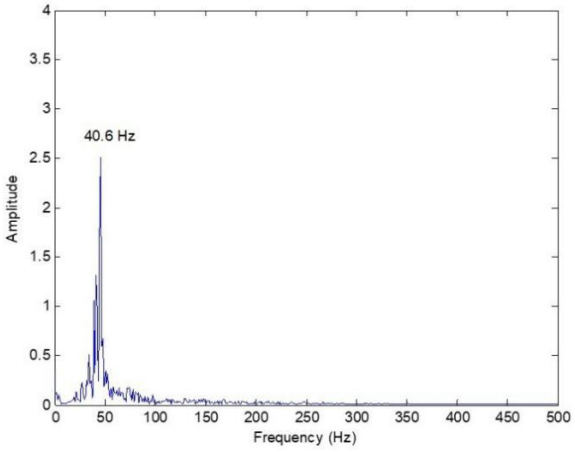

FIGURE 26. FFT analysis of the current waveforms after resonance suppression with a general filter (resonance frequency drifts).

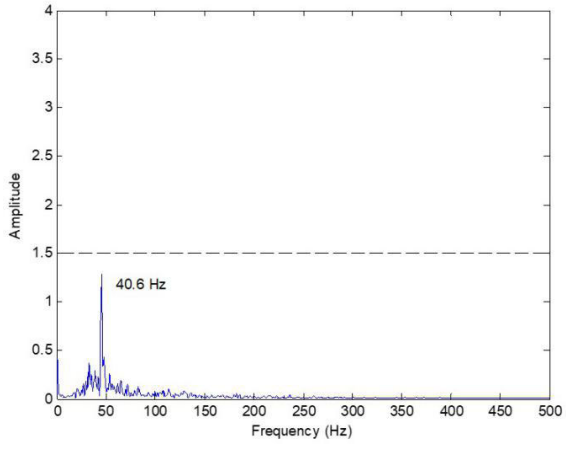

FIGURE 27. FFT analysis of the current waveforms after resonance suppression with an optimal online suppression algorithm (resonance frequency drifts).

suppress the mechanical resonance after drift in real time. The phase margin comparison is shown in Table 7.

Fig. 28 and Fig. 29 show the response curves of the quadrature axis current and speed of the servo system motor. The experimental results show that the optimal notch filter designed in this paper minimally changes the stability of the system, while the ordinary filter makes the speed and current obviously fluctuate.

TABLE 7. Comparison of the phase margins before and after resonance suppression (resonance frequency drifts).

Condition	Phase margin
Before suppression	45.1754
General filter	43.9987
Optimized filter	45.0612

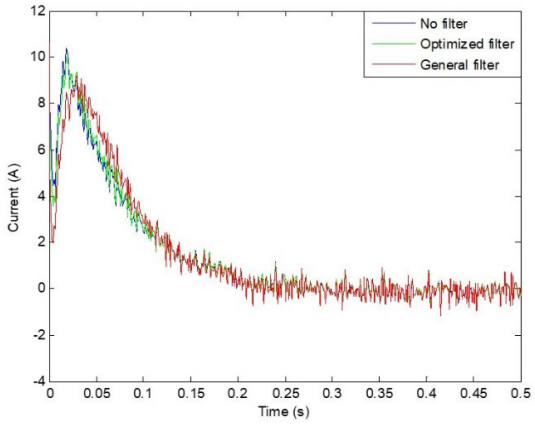

FIGURE 28. Quadrature axis current response (resonance frequency drifts).

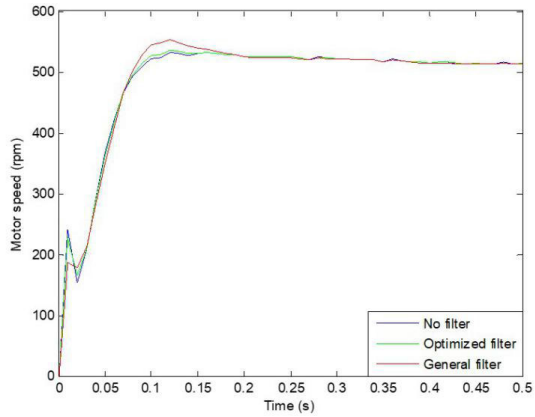

FIGURE 29. Motor speed response (resonance frequency drifts).

Experiment 3 Robust analysis of optimal online resonance suppression algorithm

Keep the parameters a and b unchanged when the inertia ratio p, stiffness coefficient k_s, viscosity damping coefficient c_s and moment of inertia of the motor J_m change. If the resonance peak value of the control system is less than the threshold H_{th} in the process of external parameter changes, and the phase margin remains in the interval [30° 70°], the system remains stable. This finding indicates that the system has strong robustness.

Fig. 30 - Fig. 37 show the curves of the resonance peak and phase margin, respectively. When $19.1 \leq p \leq 31.2$, $0.164 \leq c_s \leq 1$, $260 \leq k_s \leq 270$ and $0.00257 \leq J_m \leq 0.00437$, it is obvious that the resonance peak value is less than the threshold value H_{th} and that the phase margin is in the interval [30° 70°].

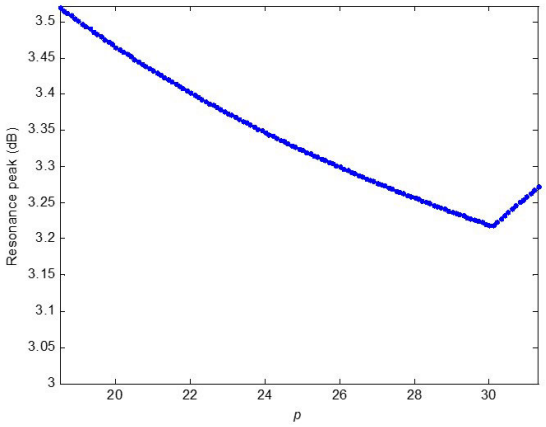

FIGURE 30. Curve of the resonance peak with different p.

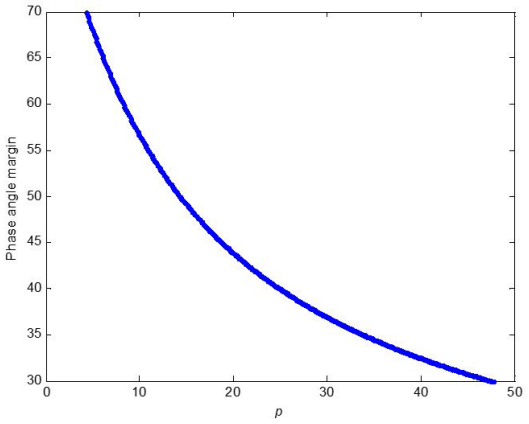

FIGURE 31. Curve of the phase margin with different p.

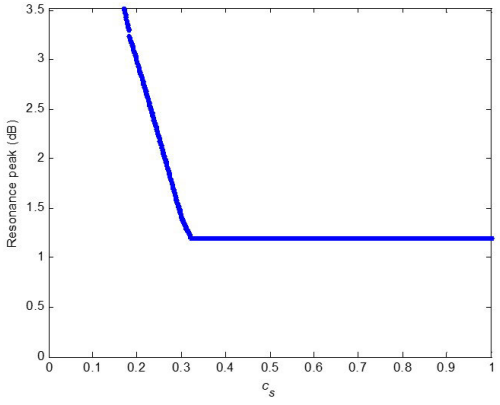

FIGURE 32. Curve of the resonance peak with different c_s.

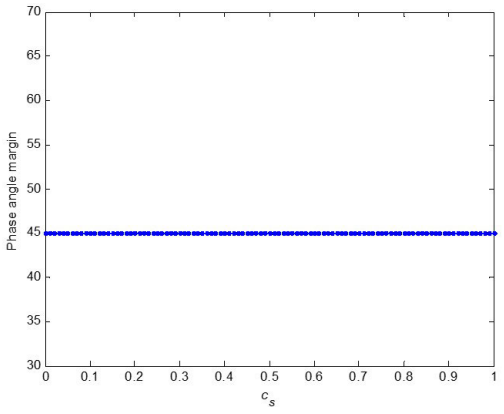

FIGURE 33. Curve of the phase margin with different c_s.

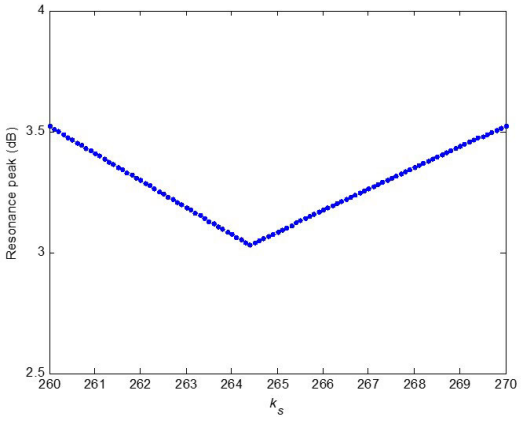

FIGURE 34. Curve of the resonance peak with different k_s.

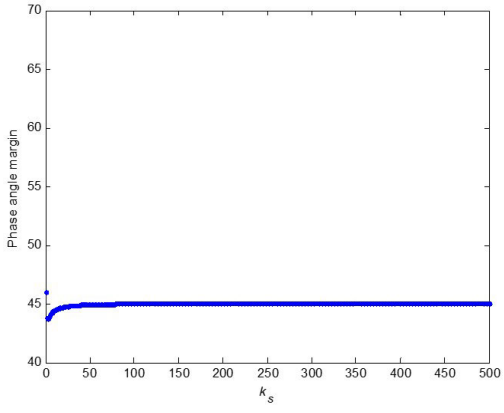

FIGURE 35. Curve of the phase margin with different k_s.

Fig. 38, Fig. 39, Fig. 40 and Fig. 41 show the motor speed response curves with p, $c_s k_s$ and J_m, respectively.

The results show that when the mechanical parameters p, c_s, and k_s and motor parameter J_m change greatly, the system still has reasonable speed response characteristics. Thus, the control system based on the proposed method has strong robustness.

The commonly utilized manual adjustment method is time-consuming, inaccurate and untimely. The aim of the online adjustment method is to search the resonant frequency online in real time via the optimal algorithm. Compared with the algorithm in literature [28], the number of iterations of the multi-frequency fast search algorithm proposed in this paper is significantly reduced, which only needs 0.45 s, with a decrease of 5 s. According to the resonant

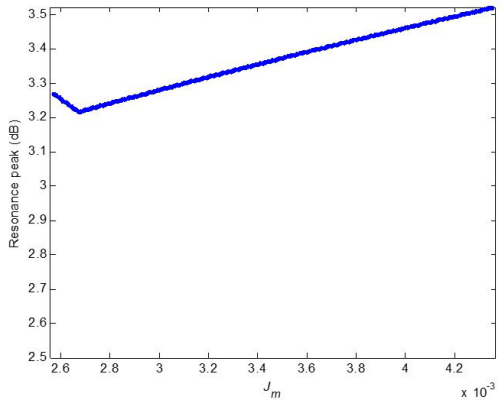

FIGURE 36. Curve of the resonance peak with different J_m.

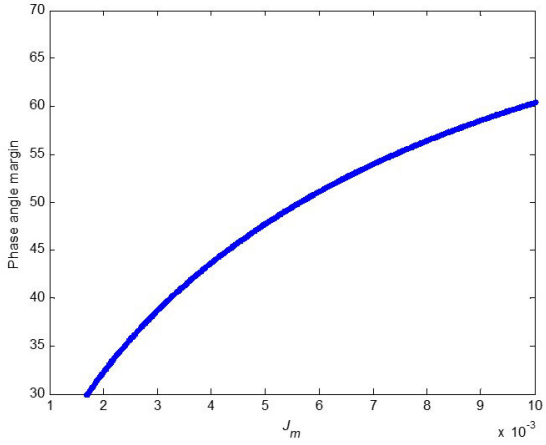

FIGURE 37. Curve of the phase margin with different k_s.

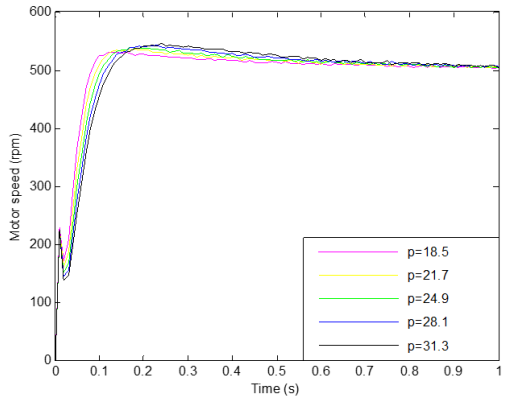

FIGURE 38. Motor speed response with different p.

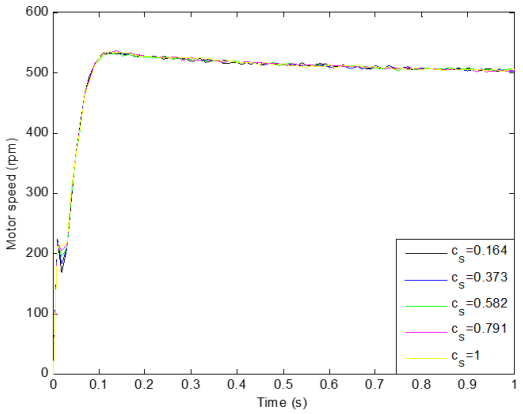

FIGURE 39. Motor speed response with different c_s.

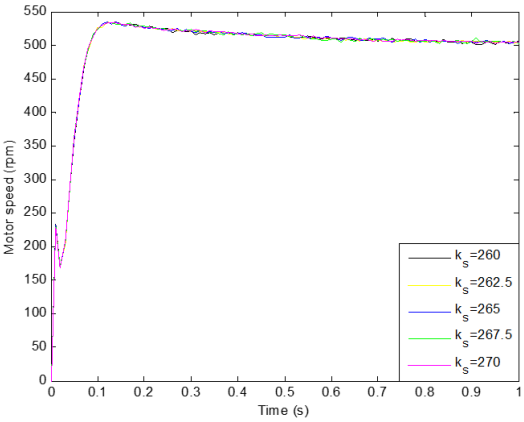

FIGURE 40. Motor speed response with different k_s.

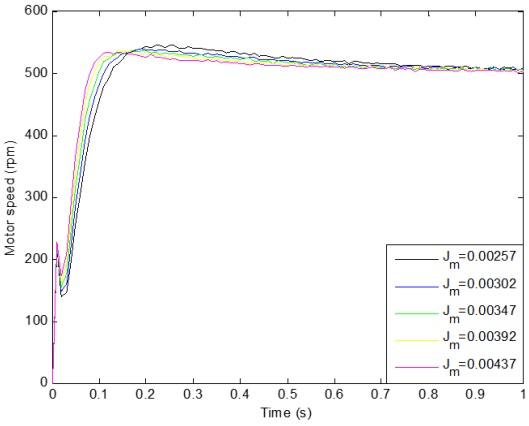

FIGURE 41. Motor speed response with different J_m.

frequency obtained from the search, the optimal algorithm is used to determine that the notch filter parameters only need 0.9 s. The whole algorithm (resonant frequency search + cutoff frequency search + drift parameter tuning + notch filter parameter determination) requires a total of 1.98 s (0.45 s+0.27 s+0.36 s+0.9 s), and the minimum phase angle loss is 0.0217 (1.2433°).

V. CONCLUSION

In this paper, an optimal online resonance suppression scheme is designed to address that the original notch filter fails when the resonance frequency drifts due to changes in the stiffness coefficient, inertia ratio and damping coefficient of the servo system. This scheme can not only effectively control the resonance system of the drift in real time but

also maintain the stability of the system. The experimental results show that the proposed multifrequency fast search algorithm is fast and accurate; the designed optimized filter can effectively suppress mechanical resonance, providing a solid theoretical basis for industrial applications.

REFERENCES

[1] X. Li, W. Zhou, J. Luo, J. Qian, W. Ma, P. Jiang, and Y. Fan, "A new mechanical resonance suppression method for large optical telescope by using nonlinear active disturbance rejection control," *IEEE Access*, vol. 7, pp. 94400–94414, Jul. 2019.

[2] M. A. Stephens, C. Manzie, and M. C. Good, "Model predictive control for reference tracking on an industrial machine tool servo drive," *IEEE Trans. Ind. Informat.*, vol. 9, no. 2, pp. 808–816, May 2013.

[3] W. Aimeng, L. Heming, S. Pengwei, W. Yi, and W. Shuting, "DSP-based field oriented control of PMSM using SVPWM in radar servo system," in *Proc. IEEE Int. Conf. Electric Mach. Drives*, Dec. 2005, pp. 486–489.

[4] T. Yuan, D. Wang, X. Wang, X. Wang, and Z. Sun, "High-precision servo control of industrial robot driven by PMSM-DTC utilizing composite active vectors," *IEEE Access*, vol. 7, pp. 7577–7587, Jan. 2019.

[5] M. Yang, H. Hu, and D.-G. Xu, "Cause and suppression of mechanical resonance in PMSM drive system," *Electr. Mach. Control*, vol. 16, no. 1, pp. 79–84, Jan. 2012.

[6] Y. Yang, J.-M. Zhang, G.-Q. Xu, S. Wang, and F. Wang, "Application research on speed negative feedback in mechanical resonance suppression in servo system," *Trans China Electrotech. Soc.*, vol. 33, no. 23, pp. 5459–5469, Dec. 2018.

[7] T. Orlowska-Kowalska and K. Szabat, "Control of the drive system with stiff and elastic couplings using adaptive neuro-fuzzy approach," *IEEE Trans. Ind. Electron.*, vol. 54, no. 1, pp. 228–240, Feb. 2007.

[8] T. Orlowska-Kowalska and K. Szabat, "Damping of torsional vibrations in two-mass system using adaptive sliding neuro-fuzzy approach," *IEEE Trans. Ind. Informat.*, vol. 4, no. 1, pp. 47–57, Feb. 2008.

[9] S.-M. Lee and B. S. Park, "Robust control for trajectory tracking and balancing of a ballbot," *IEEE Access*, vol. 8, pp. 159324–159330, Aug. 2020.

[10] T. Orlowska-Kowalska, M. Kaminski, and K. Szabat, "Implementation of a sliding-mode controller with an integral function and fuzzy gain value for the electrical drive with an elastic joint," *IEEE Trans. Ind. Electron.*, vol. 57, no. 4, pp. 1309–1317, Apr. 2010.

[11] H. Zoubek and M. Pacas, "Encoderless identification of two-mass-systems utilizing an extended speed adaptive observer structure," *IEEE Trans. Ind. Electron.*, vol. 64, no. 1, pp. 595–604, Jan. 2017.

[12] Y. Wu, N. Sun, H. Chen, and Y. Fang, "Adaptive output feedback control for 5-DOF varying-cable-length tower cranes with cargo mass estimation," *IEEE Trans. Ind. Informat.*, vol. 17, no. 4, pp. 2453–2464, Apr. 2021.

[13] S. H.-H. Zhao, Y.-L. Mao, C.-C. Xu, and Y.-S. H. Chen, "Torsional vibration suppression based on adaptive observer and linear quadratic regulator in high performance servo drives," *Trans. China Electrotech. Soc.*, vol. 31, no. 6, pp. 108–117, Mar. 2016.

[14] X. Kestelyn and E. Semail, "A vectorial approach for generation of optimal current references for multiphase permanent-magnet synchronous machines in real time," *IEEE Trans. Ind. Electron.*, vol. 58, no. 11, pp. 5057–5065, Nov. 2011.

[15] R. Dhaouadi, K. Kubo, and M. Tobise, "Analysis and compensation of speed drive systems with torsional loads," *IEEE Trans. Ind. Appl.*, vol. 30, no. 3, pp. 760–766, May/Jun. 1994.

[16] X. Liu, H. Yu, J. Yu, and L. Zhao, "Combined speed and current terminal sliding mode control with nonlinear disturbance observer for PMSM drive," *IEEE Access*, vol. 6, pp. 29594–29601, May 2018.

[17] B. S. Umesh and K. Sivakumar, "Multilevel inverter scheme for performance improvement of pole-phase-modulated multiphase induction motor drive," *IEEE Trans. Ind. Electron.*, vol. 63, no. 4, pp. 2036–2043, Apr. 2016.

[18] X. Lei, D. Zhang, and Y. Jin, "Research on vibration suppression of the forklift steering system based on finite element modal analysis and pole placement," in *Proc. IEEE Int. Symp. Robot. Manuf. Autom. (ROMA)*, Kuala Lumpur, Malaysia, Dec. 2014, pp. 46–51.

[19] S. Thomsen, N. Hoffmann, and F. W. Fuchs, "PI control, PI-based state space control, and model-based predictive control for drive systems with elastically coupled loads—A comparative study," *IEEE Trans. Ind. Electron.*, vol. 58, no. 8, pp. 3647–3657, Aug. 2011.

[20] T. M. O'Sullivan, C. M. Bingham, and N. Schofield, "High-performance control of dual-inertia servo-drive systems using low-cost integrated SAW torque transducers," *IEEE Trans. Ind. Electron.*, vol. 53, no. 4, pp. 1226–1237, Jun. 2006.

[21] S. E. Saarakkala and M. Hinkkanen, "Identification of two-mass mechanical systems using torque excitation: Design and experimental evaluation," *IEEE Trans. Ind. Appl.*, vol. 51, no. 5, pp. 4180–4189, Sep. 2015.

[22] S. Brock, D. Luczak, K. Nowopolski, T. Pajchrowski, and K. Zawirski, "Two approaches to speed control for multi-mass system with variable mechanical parameters," *IEEE Trans. Ind. Electron.*, vol. 64, no. 4, pp. 3338–3347, Apr. 2017.

[23] S. Chen, G. Liu, and S. Zheng, "Sensorless control of BLDCM drive for a high-speed maglev blower using low-pass filter," *IEEE Trans. Power Electron.*, vol. 32, no. 11, pp. 8845–8856, Nov. 2017.

[24] C. Peng, J. Sun, C. Miao, and J. Fang, "A novel cross-feedback notch filter for synchronous vibration suppression of an MSFW with significant gyroscopic effects," *IEEE Trans. Ind. Electron.*, vol. 64, no. 9, pp. 7181–7190, Sep. 2017.

[25] D. H. Lee, J. H. Lee, and J. W. Ahn, "Mechanical vibration reduction control of two-mass permanent magnet synchronous motor using adaptive notch filter with fast Fourier transform analysis," *IET Electr. Power Appl.*, vol. 6, no. 7, pp. 455–461, 2012.

[26] M. Yang, L. Hao, and D.-G. Xu, "Analysis of mechanical resonance mechanism and fast identification of resonance characteristic for two-mass system with elastic load," *Electr. Mach. Control*, vol. 20, no. 4, pp. 112–120, Apr. 2016.

[27] J.-M. Wang, Y.-D. Wu, Y.-M. Liu, and W.-L. Zhang, "Resonance suppression of servo system based on digital filter," *J. Beijing Univ. Aeronaut. Astronaut.*, vol. 41, no. 3, pp. 485–491, Mar. 2015.

[28] Y. Xiong and Y.-S. Li, "Servo control strategy for resonance suppression based on searching for frequency characteristic," *Electr. Drive*, vol. 45, no. 2, pp. 39–44, Feb. 2015.

JIAKUAN XIA received the B.S., M.S., and Ph.D. degrees in electrical engineering from the Shenyang University of Technology, China, in 1986, 1997 and 2006, respectively. He is currently a Professor with the School of Electrical Engineering, Shenyang University of Technology. His research interests include artificial intelligence and modern motion control, power electronics and power transmission, large synchronous motor excitation system design and research, and special motor design and control.

ZHIYAN GUO received the B.S. degree in electrical automatization from the School of Nanchang University, Nanchang, China, in 2007, and the M.S. degree in electrical engineering from Northeast University, Shenyang, China, in 2014. He is currently pursuing the Ph.D. degree with the School of Electrical Engineering, Shenyang University of Technology, China. His research interests include high-precision servo systems in machine tools, vibration abatement, and motion control systems.

ZEXING LI received the B.S. degree in electrical automatization from the School of Shenyang University of Technology, Shenyang, China, in 2017. He is currently pursuing the M.S. and Ph.D. degrees with the School of Electrical Engineering, Shenyang University of Technology. His research interest includes motor design and control.